

# Influence of synthetic method on the properties of $\text{La}_{0.5}\text{Ba}_{0.5}\text{FeO}_3$ SOFC cathode

A. Ecija <sup>1</sup>, K. Vidal <sup>1</sup>, A. Larrañaga <sup>1</sup>, L. Ortega-San-Martín <sup>2</sup> and M. I. Arriortua <sup>1</sup>

<sup>1</sup> Universidad del País Vasco (UPV/EHU), Facultad de Ciencia y Tecnología,  
Departamento de Mineralogía y Petrología, Barrio Sarriena S/N, 48940 Leioa,  
Vizcaya, Spain.

<sup>2</sup> Pontificia Universidad Católica del Perú (PUCP), Dpto. Ciencias, Sección  
Químicas. Av. Universitaria 1801. Lima-32, Perú.



Universidad  
del País Vasco

Euskal Herriko  
Unibertsitatea



## Contents:

- **Introduction**
  - Solid oxide fuel cells
  - Perovskites
- **Experimental preparation**
  - Solid state reaction
  - Glycine nitrate combustion process
- **Characterization**
  - Structure (X-ray and neutron diffraction )
  - Microstructure
  - Bulk conductivity
  - Thermal expansion coefficient
  - Polarization resistance
- **Conclusions**
- **Acknowledgments**

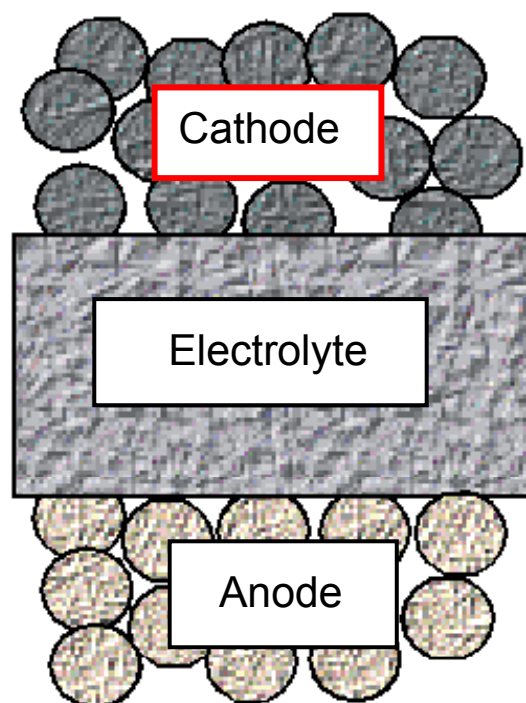


# 5

# Introduction

Perovskites  $\text{Ln}_{1-x}\text{M}_x\text{BO}_3$   
 $\text{Ln}$  = trivalent lanthanide  
 $\text{M}$  = divalent alkaline-earth cations  
 $\text{B}$  = transition metal

## Materiales



Perovskite  $\text{ABO}_3$  with YSZ or SDC (samaria doped ceria) composite

Yttria doped zirconia YSZ

Nickel-YSZ cermet

### Electrical properties

Conductivity  
( $\sigma_{\text{el}} + \sigma_{\text{ion}}$ )

Catalytic activity

Ionic conductivity  
( $\sigma_{\text{ion}} >> \sigma_{\text{el}}$ )

Catalytic activity  
Conductivity  
( $\sigma_{\text{el}} + \sigma_{\text{ion}}$ )

### Thermomechanical properties

Porosity  
Thermal expansion coefficient (TEC)

Adhesion

Gas-tightness  
Mechanical stability

Adhesion  
Thermal expansion coefficient (TEC)  
Porosity

### Stability

Under reducing atmospheres

Under reducing and oxidizing atmospheres

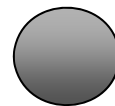
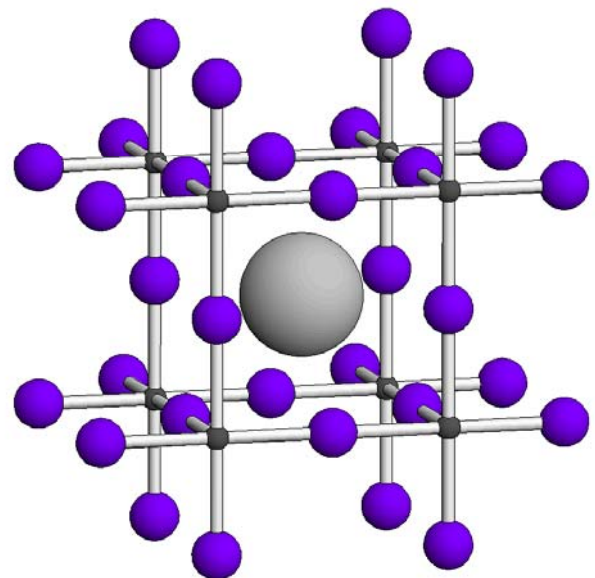
Under oxidizing atmospheres





# Perovskites

## Introduction



A ( $\text{Ln}^{3+}$ ,  $\text{M}^{2+}$ )



O



B (Fe, Mn, Co)

Parameters that control the A position of the perovskite

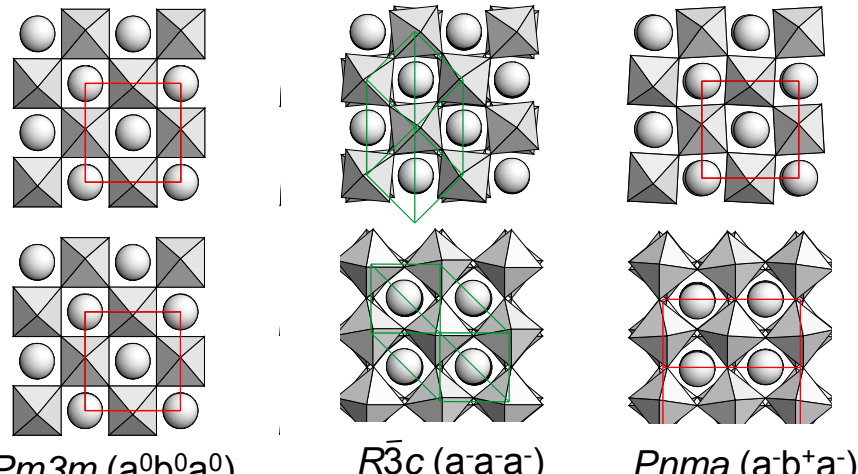
**Tolerance factor (Goldschmidt)**

Define the stability of perovskites

$$t = \frac{(r_A + r_O)}{2^{\frac{1}{2}} \cdot (r_B + r_O)}$$

**Ideal perovskite**  
 $t = 1$

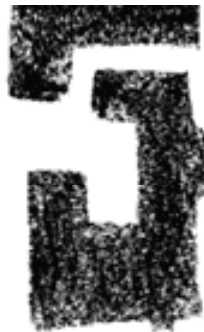
**Non-ideal perovskite**  
 $t \neq 1$



Perfect adjustment  
between the sizes of the atoms that form  
the structure

Mismatch





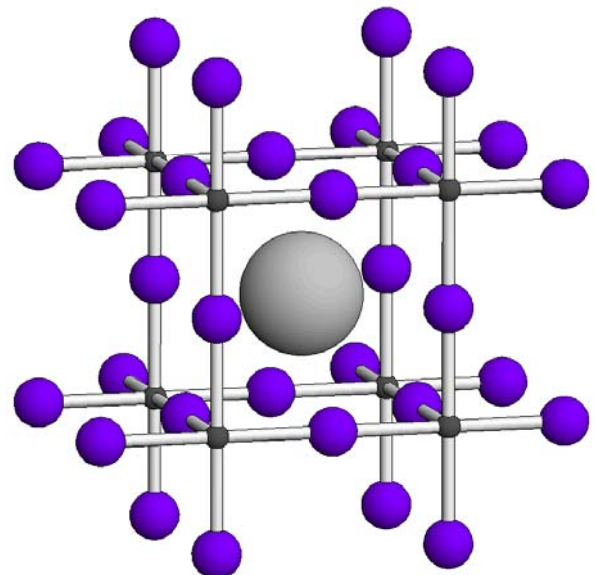
# Perovskites

# Introduction

Parameters that control the A position of the perovskite

**Tolerance factor (Goldschmidt)**

Define the stability of perovskites



● A ( $\text{Ln}^{3+}$ ,  $\text{M}^{2+}$ )

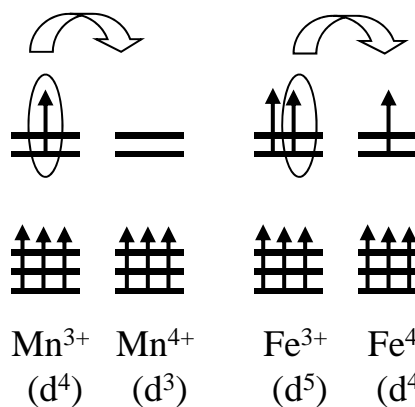
● O

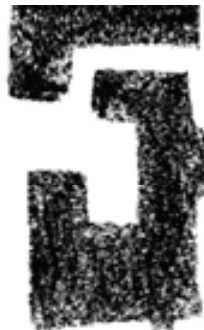
● B (Fe, Mn, Co)

$$t = \frac{(r_A + r_O)}{2^{\frac{1}{2}} \cdot (r_B + r_O)}$$

$t = 1$  Ideal perovskite  
 $t \neq 1$  Non-ideal perovskite

Hole doping level  $x$





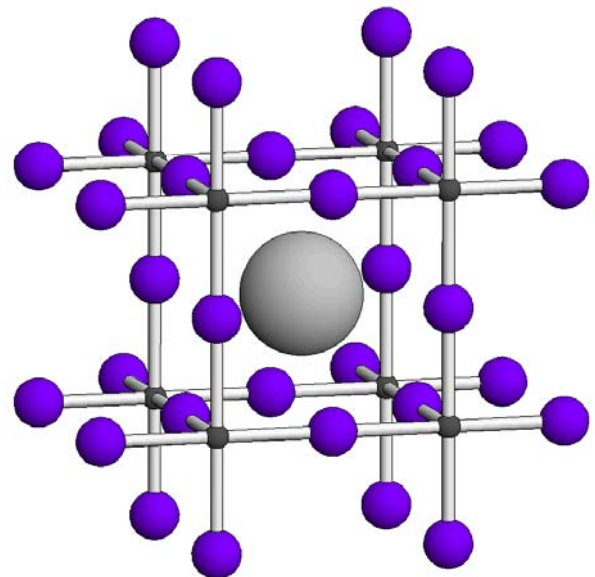
# Perovskites

# Introduction

Parameters that control the A position of the perovskite

**Tolerance factor (Goldschmidt)**

Define the stability of perovskites



● A ( $\text{Ln}^{3+}, \text{M}^{2+}$ )

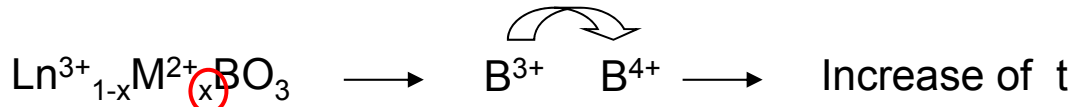
● O

● B (Fe, Mn, Co)

$$t = \frac{(r_A + r_O)}{2^{\frac{1}{2}} \cdot (r_B + r_O)}$$

↑ ↑  
 $t = 1$       Ideal perovskite  
 $t \neq 1$       Non-ideal perovskite

**Hole doping level x**

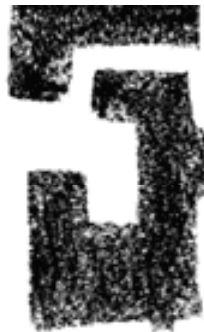


**Mean ionic radius  $\langle r_A \rangle$**

$$\langle r_A \rangle = \sum_i y_i \cdot r_i$$

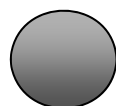
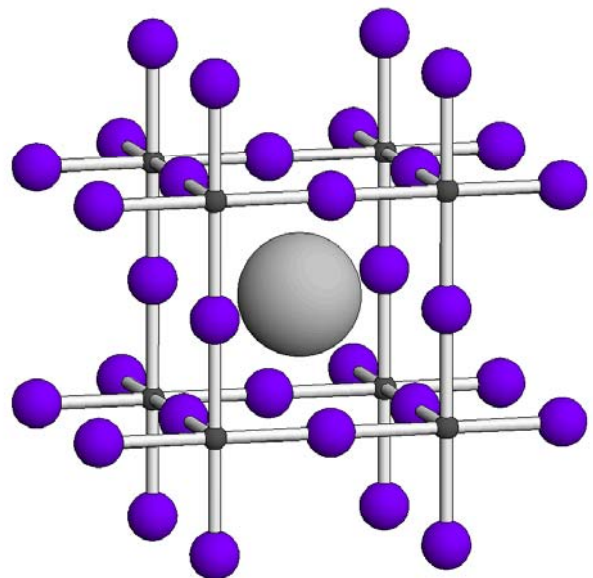
$\langle r_A \rangle$  increases  $\longrightarrow$  increase of t





# Perovskites

# Introduction



A ( $\text{Ln}^{3+}$ ,  $\text{M}^{2+}$ )



O



B (Fe, Mn, Co)

Parameters that control the A position of the perovskite

**Tolerance factor (Goldschmidt)**

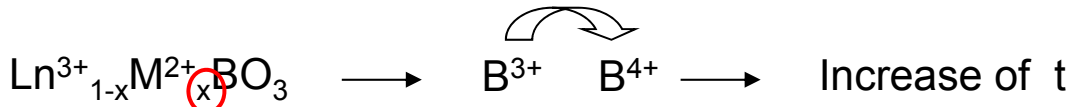
Define the stability of perovskites

$$t = \frac{(r_A + r_O)}{2^{\frac{1}{2}} \cdot (r_B + r_O)}$$

↑                           ↑

$t = 1$       Ideal perovskite  
 $t \neq 1$       Non-ideal perovskite

**Hole doping level x**



**Mean ionic radius  $\langle r_A \rangle$**

$$\langle r_A \rangle = \sum_i y_i \cdot r_i$$

$\langle r_A \rangle$  increases  $\longrightarrow$  increase of t

**A cation size disorder A  $\sigma^2(r_A)$**

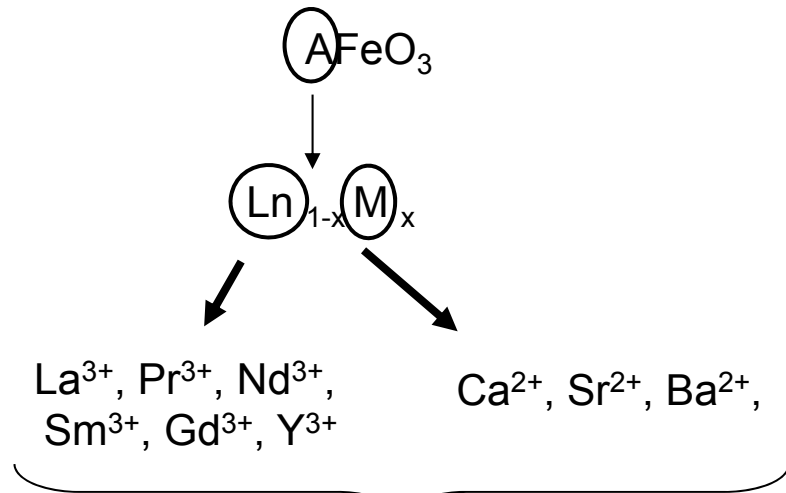
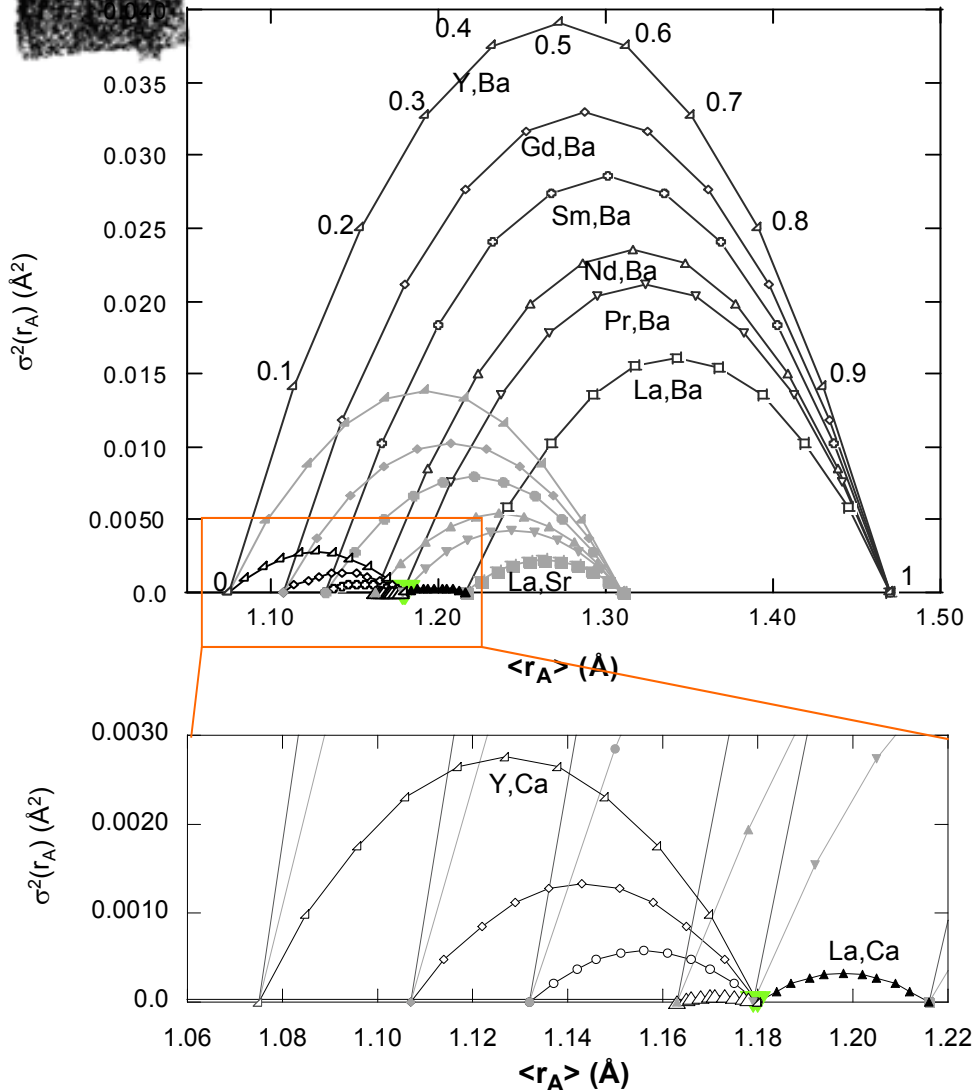
$$\sigma^2 \langle r_A \rangle = \langle r_A^2 \rangle - \langle r_A \rangle^2$$





# Perovskites

# Introduction



An extremely wide variety  
of combinations of chemical elements

Stable phases  
Interesting properties





# Perovskites

## Introduction

### Focus of research

In this research, a  $\text{La}_{0.5}\text{Ba}_{0.5}\text{FeO}_3$  perovskite has been synthesized by these two different methods (ceramic and glycine-nitrate routes) in order to study the synthetic method influence on the properties of this compound as IT-SOFC cathode material.

This composition has been chosen due to its **intermediate hole doping level** (0.5) and **high average size of the A-site cations** ( $\langle r_A \rangle = 1.48 \text{ \AA}$ , where  $r_A$  are standard 12-coordinate ionic radii) that according with previous studies should show interesting properties for its use as **SOFC cathode**.

R.D. Shannon, Acta Cryst, 1976, A32, 751-767.

G. Ch. Kostogloudis, Ch. Ftikos, J. European Ceram. Soc., 19 (1999) 497-505.

K. Vidal, L.M. Rodríguez-Martínez, L. Ortega San-Martín, A. Martínez-Amesti, M.L. Núñez, T. Rojo, A. Laresgoiti, M.I. Arriortua, J. Power Sources, 92 (2009) 175-179.

A. Ecija, K. Vidal, A. Larrañaga, A. Martínez-Amesti, L. Ortega-San-Martín, M. I. Arriortua, Solid State Ionics, 201(1) (2011) 35-41.

L. Jia, X. Wang, W. Li, K. Li, B. Chi, J. Pu, L. Jian, S. Yuan, J. Power Sources, 253 (2014) 138-142.

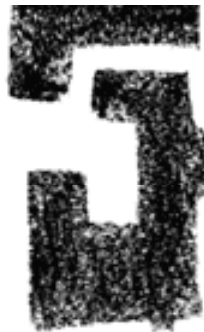




## Contents:

- **Introduction**
  - Solid oxide fuel cells
  - Perovskites
- **Experimental preparation**
  - Solid state reaction
  - Glycine nitrate combustion process
- **Characterization**
  - Structure (X-ray and neutron diffraction )
  - Microstructure
  - Bulk conductivity
  - Thermal expansion coefficient
  - Polarization resistance
- **Conclusions**
- **Acknowledgments**





## Solid state reaction

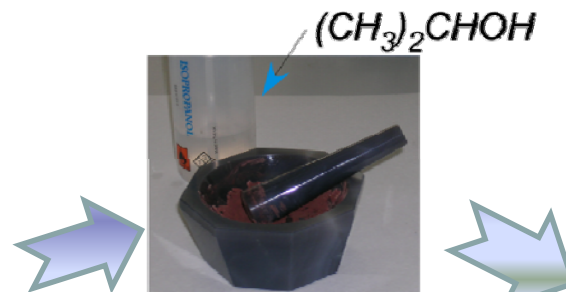
Stoichiometric amounts of oxides of the corresponding elements were mixed in an agate mortar



$Fe_2O_3$



$La_2O_3$

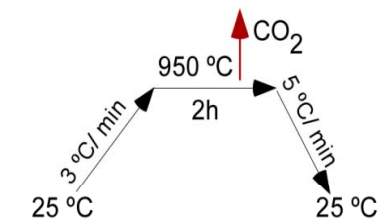


The powder was weighed and then manually grinded in an agate mortar with isopropanol for homogenization

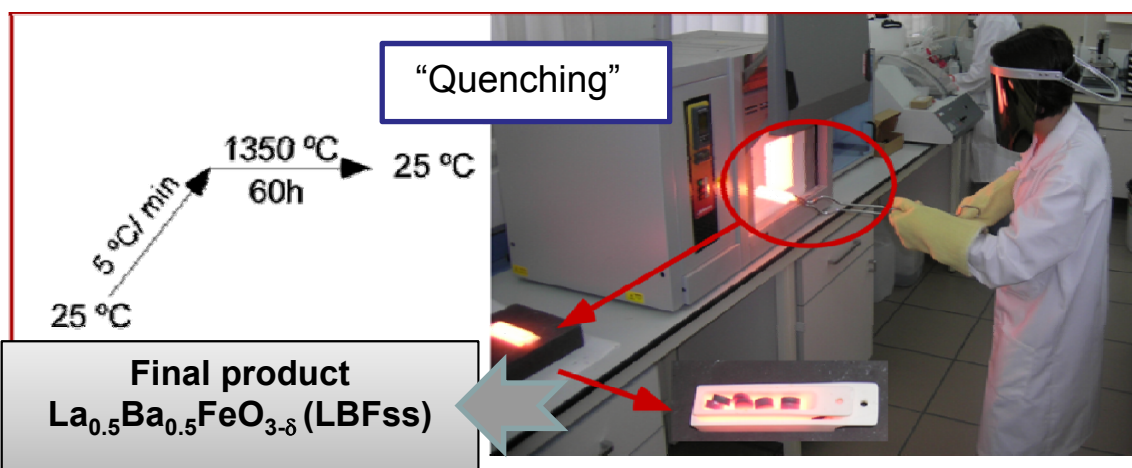


## Experimental preparation

The mixture was calcined in air at 950°C (2h)

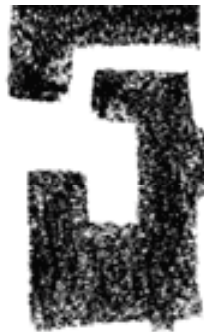


The product obtained was ground, pelletized again, fired at 1350°C for 60h and rapidly cooled to room temperature ("quenching")



Final product  
 $La_{0.5}Ba_{0.5}FeO_{3-\delta}$  (LBFss)





# Glycine nitrate combustion process

## Experimental preparation

Metal nitrates were dissolved in distilled water



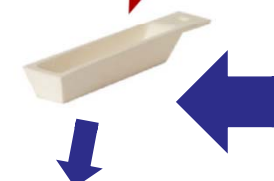
Glycine/nitrate molar ratio of 2:1



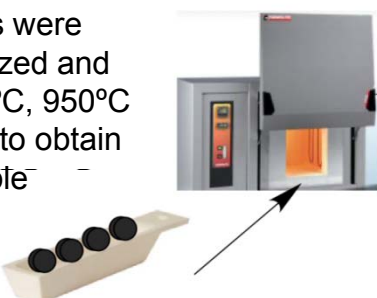
Resulting viscous liquid autoignited at about 400°C

Viscous gel

Combustion  
~ 400°C



Obtained powders were subsequently pelletized and calcined in air at 850°C, 950°C and 1050°C for 10 h to obtain the pure sample



Calcined in air at 800°C for 2 hours

25 °C

3 °C/min

800 °C

2h

CO<sub>2</sub>

25 °C

5 °C/min



Precursor powders

Final product  
 $\text{La}_{0.5}\text{Ba}_{0.5}\text{FeO}_{3-\delta}$  (LBFgn)

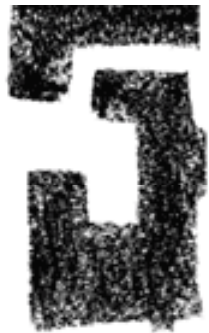




## Contents:

- **Introduction**
  - Solid oxide fuel cells
  - Perovskites
- **Experimental preparation**
  - Solid state reaction
  - Glycine nitrate combustion process
- **Characterization**
  - Structure (X-ray and neutron diffraction )
  - Microstructure
  - Bulk conductivity
  - Thermal expansion coefficient
  - Polarization resistance
- **Conclusions**
- **Acknowledgments**



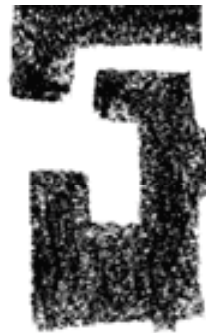


## Inductively coupled plasma atomic emission spectroscopy (ICP-AES)

### Characterization

Compound	Nominal composition	Experimental composition		
		La	Ba	Fe
LBFss	$\text{La}_{0.5}\text{Ba}_{0.5}\text{FeO}_3$	0.48(3)	0.52(2)	1.00(1)
LBFgn	$\text{La}_{0.5}\text{Ba}_{0.5}\text{FeO}_3$	0.49(2)	0.51(2)	1.00(1)

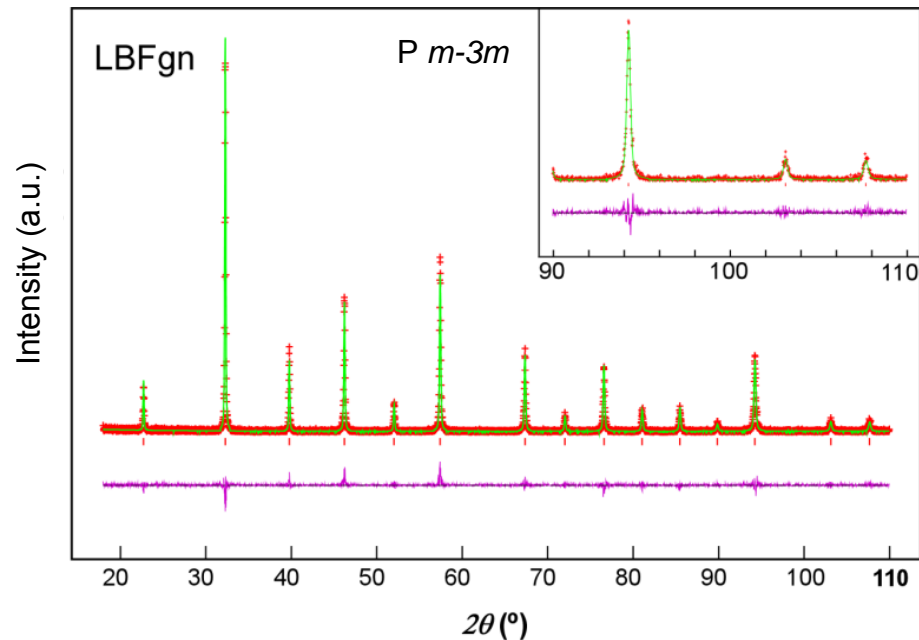
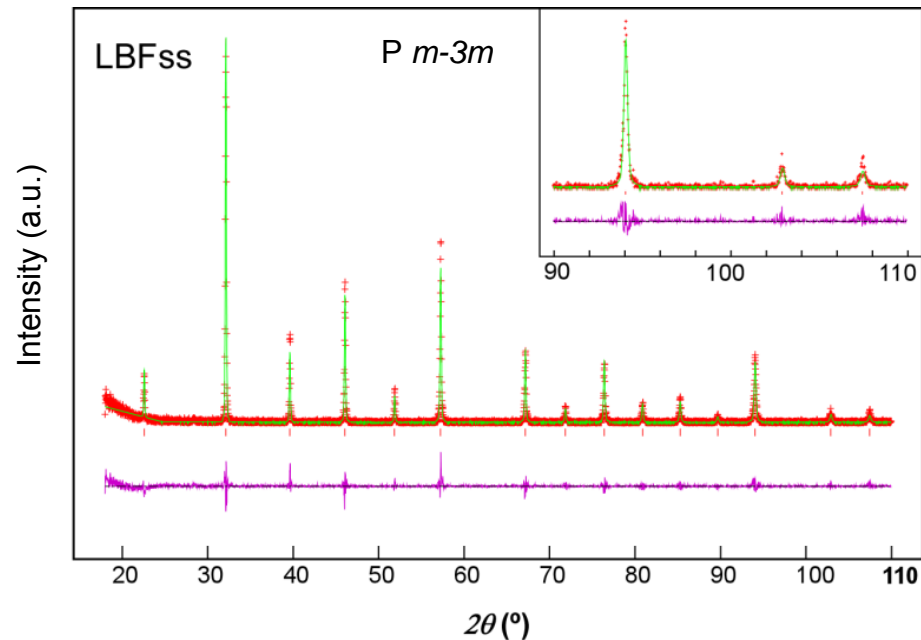
Results from chemical analyses show a good agreement between the analyzed chemical compositions of the prepared powders and the nominal compositions.



# Difracción de Rayos X (DRX)

## Characterization

Rietveld method, program GSAS.



Results on the Rietveld analysis of these powder diffraction patterns show cubic symmetry ( $P\ m\bar{3}m$ ) for the samples.

H. M. Rietveld, J. Appl. Crystallogr., 2 (1969) 65-71.

Larson A.C., Von Dreele R.B., "GSAS: General Structure Analysis System", LAUR, 86, 1994.



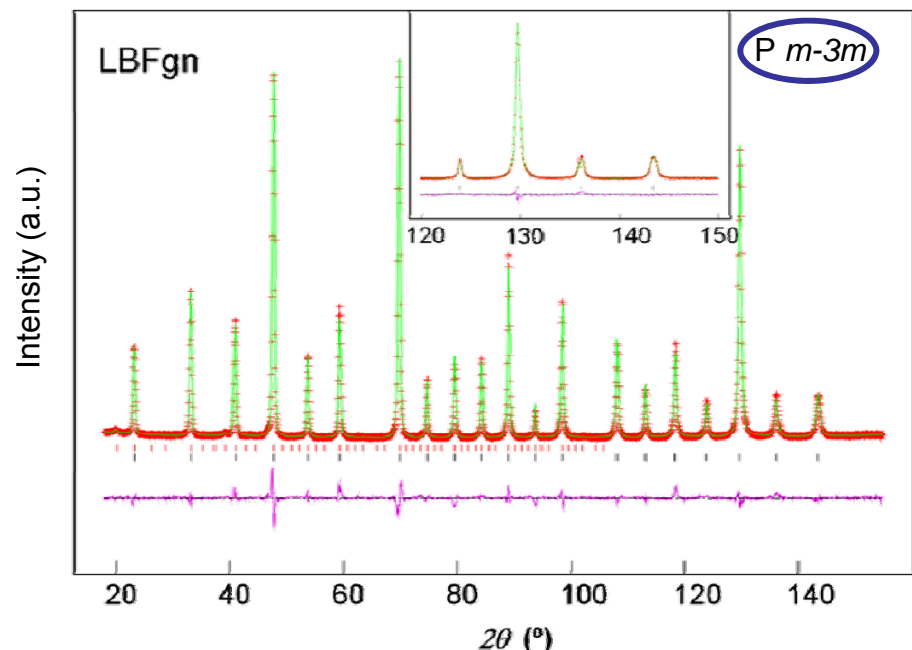
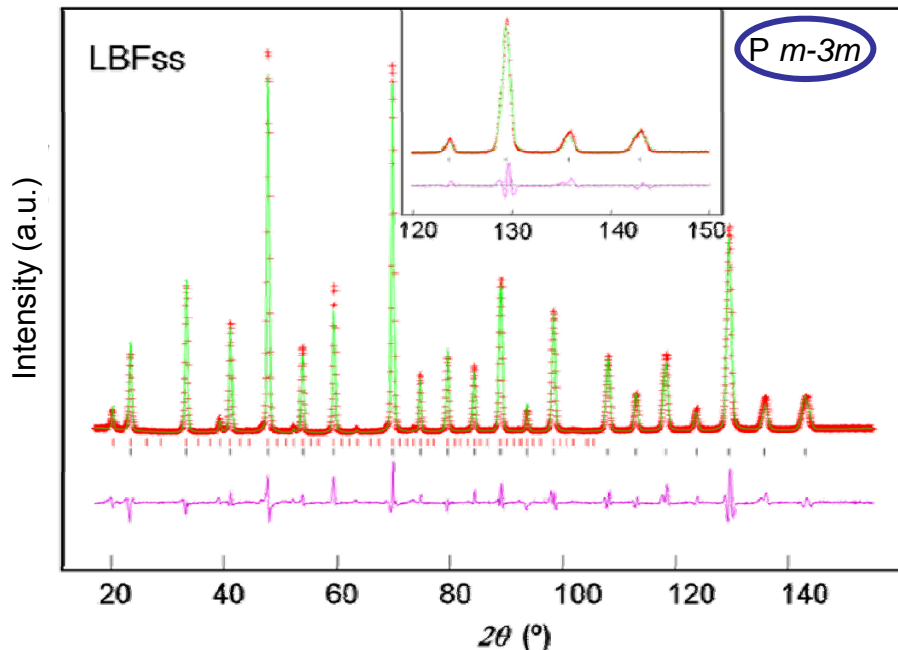


# High-resolution neutron powder diffraction

## Characterization

Rietveld method, program GSAS (considering a G-type magnetic structure).

Neutron powder diffraction data collected with D2B diffractometer of the Institute Laue-Langevin.



Neutron diffraction measurements were performed in order to obtain information about the oxygen stoichiometry and to clarify the crystal structure of both phases. Structure refinements were carried out by fitting simultaneously the X-ray and neutron diffraction data.

H. M. Rietveld, J. Appl. Crystallogr., 2 (1969) 65-71.

Larson A.C., Von Dreele R.B., "GSAS: General Structure Analysis System", LAUR, 86, 1994.





# High-resolution neutron powder diffraction

## Characterization

Compound	a(Å)	V(Å³)	$\rho_{\text{teórica}}$ (g/cm³)	d<A-Fe> (Å)	d<A-O> (Å)	d(Fe-O) (x6) (Å)
LBFss	3.9392(3)	61.12(1)	6.536	3.4114(2)	2.7854(4)	1.9696(1)
LBFgn	3.9381(1)	61.07(1)	6.568	3.4105(1)	2.7847(1)	1.9690(1)

Compound	O occupancy	3- $\delta$
LBFss	0.971(3)	2.91(1)
LBFgn	0.992(4)	2.98(1)

The main difference is observed in the oxygen stoichiometry.



Differences in cooling rates.

Fast cooling of the powder sample leads to an increase of the mole ratio of Fe<sup>3+</sup> and oxygen vacancies.

This is due to the time is not enough for all oxygen vacancies were filled and therefore, the iron cation was mostly kept in a lower valance state (Fe<sup>3+</sup>).

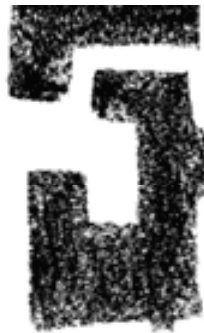
X.D. Zhou, Q. Cai, J. Yang, W.J. Yelon , W.J. James, H.U. Anderson, Solid State Ionics, 175 (2004) 83-86.

J.B. Yang, W.B. Yelan, W.J. James, Phys. rev. B, 66 (2002) 184415-1-184415-9.

K.S. Roh, K.H. Ryu, C.H. Yo, J. Mater. Sci., 30 (1995) 1245-1250.

L.Ge, Z. Zhu, Z. Shao, S. Wang, S. Liu, Ceram. Inter., 35 (2009) 3201-3206.

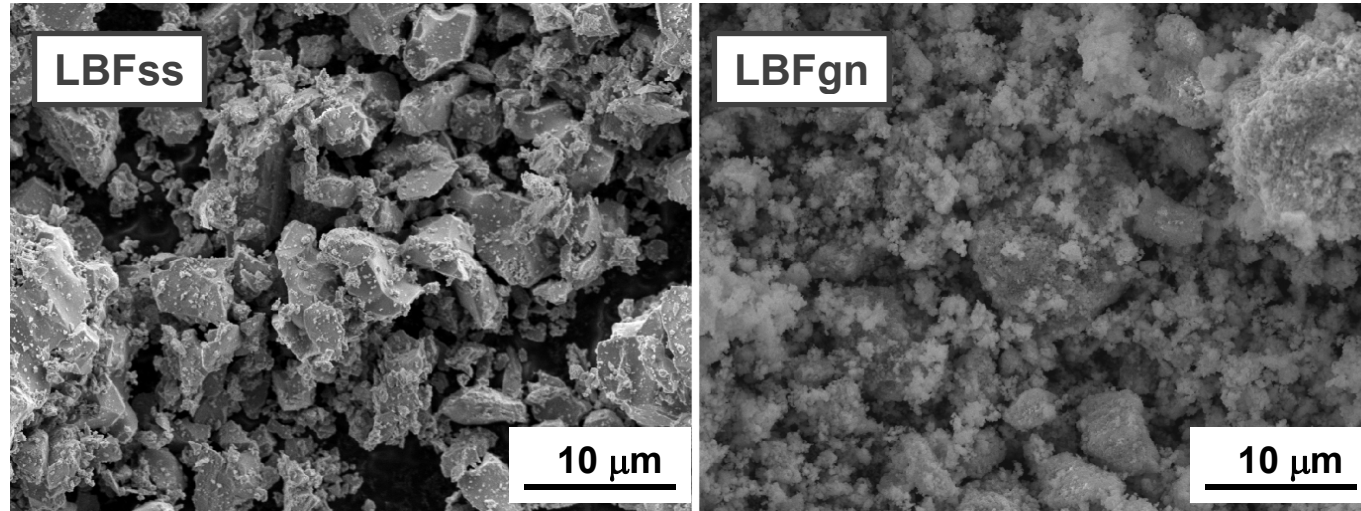




## Morphological study

## Characterization

Scanning Electron Microscope (SEM).



- Microstructure with heterogeneous grain sizes (from ~ 0.5 to 4  $\mu\text{m}$ ) and shapes.



- Particles of grain sizes about 150 nm forming agglomerates.

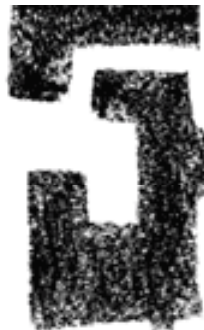
The higher calcination temperature at which is formed and longer reaction time of the ceramic process can explain the bigger grain size .

M.E. Melo Jorge, A. Correia dos Santos, M.R. Nunes, Inter. J. Inorg. Mater., 3 (2001) 915-921.

S. Li , Z. Lu, X. Huang, B. Wei, W. Su, J. Physics. Chem. Solids, 68 (2007) 1707-1712.

A. Ecija, K. Vidal, A. Larrañaga, L. Ortega-San-Martín, M.I. Arriortua: "Synthetic Methods for Perovskite Materials. Structure and Morphology", Advances in Crystallization Processes, Dr. Yitzhak Mastai (Ed.), ISBN: 978-953-51-0581-7, 2012.

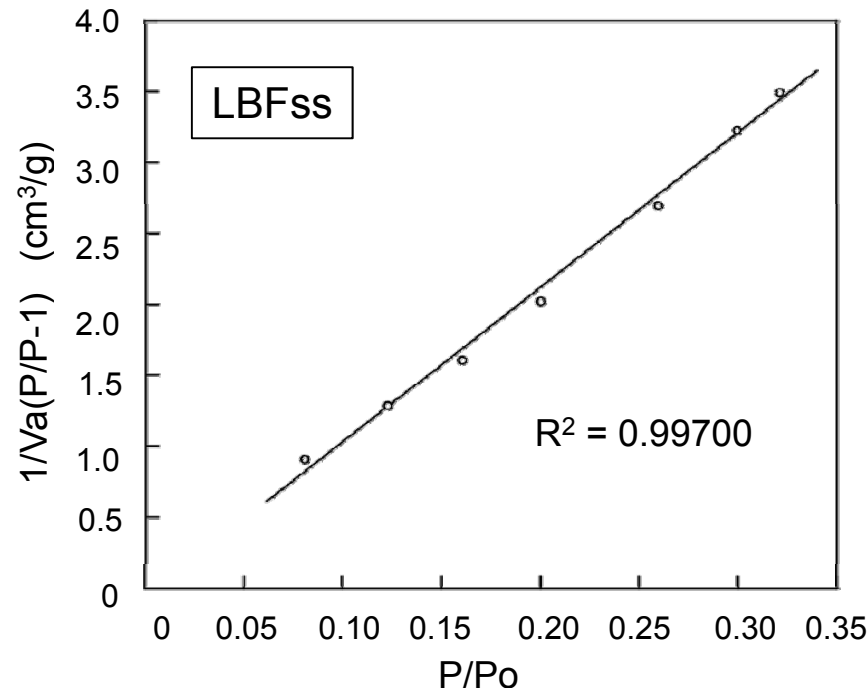




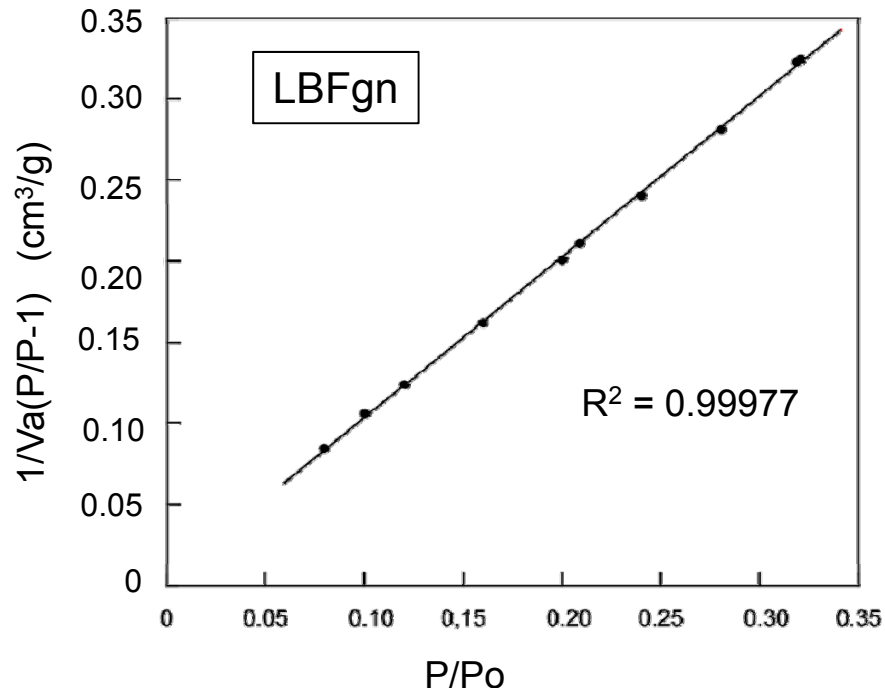
## BET Surface Area

## Characterization

Brunauer-Emmett-Teller nitrogen adsorption (BET) method.



$$S_{BET} \text{ LBFss} : 0.44 \text{ m}^2 \cdot \text{g}^{-1}$$



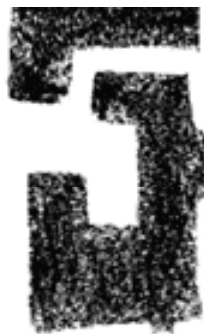
$$S_{BET} \text{ LBFgn} : 4.26 \text{ m}^2 \cdot \text{g}^{-1}$$

The glycine-nitrate method leads to powders with significant larger surface areas than the solid state reaction.

S. Brunauer, P.H. Emmet, E. Teller, J. Am. Chem. Soc., 60 (1938) 309-319.

S. Nakayama , J. Mater. Sci., 36 (2001) 5643-5648.

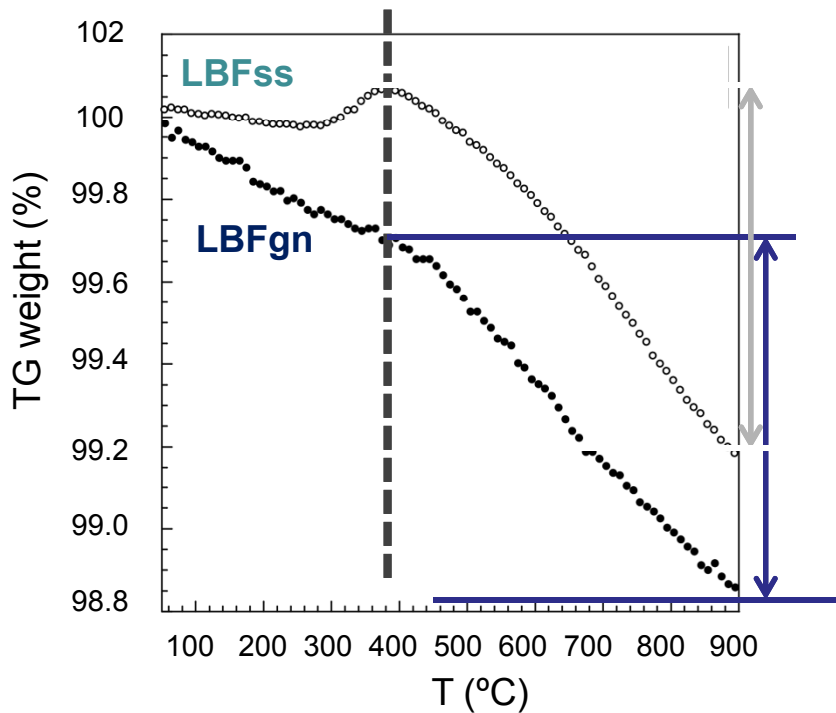




# Thermogravimetric analysis

## Characterization

The samples were heated up to 900°C at 5°C/min, under continuous flow of air.



Partial re-oxidation of  $\text{Fe}^{3+}$  to  $\text{Fe}^{4+}$  and the recovery of some of the oxygen content (~0.3%) that was lost during the quenching of the sample (265-400°C).

Sample continues losing oxygen (~0.75 %) from ~ 600°C.

Slight weight loss in air (~0.4%) from 25°C to about 470°C which is attributed to desorption of physically absorbed water and carbon dioxide.

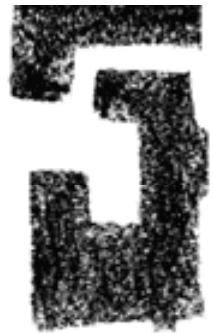
The weight of the sample starts to decrease from 470°C and continuously decreases (0.82%) up to 900°C .

Therefore, despite the higher non-stoichiometry of LBFss at room temperature, both samples have similar oxygen content at high temperatures.

W. Zhu, Z. Lü, S. Li; B. Wei, J. Miao, X. Huang, K. Chen, N. Ai, W. Su, J. Alloys Compd., 465 (2008) 274-279.

X.D. Zhou, Q. Cai, J. Yang, W.B. Yelon, W.J. James, H.U. Anderson, Solid State Ionics, 175 (2004) 83-86.

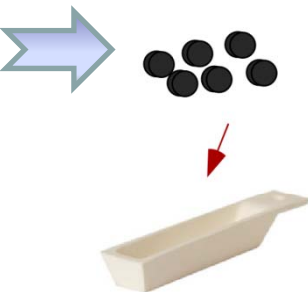




## Electrical conductivity

## Characterization

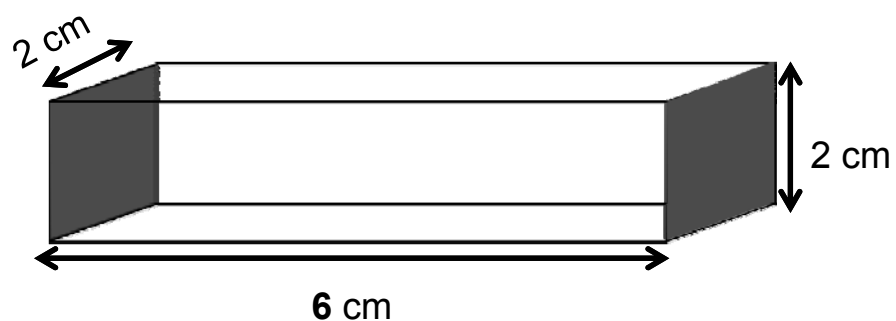
Powders of  
the samples



Sintered at 1350°C

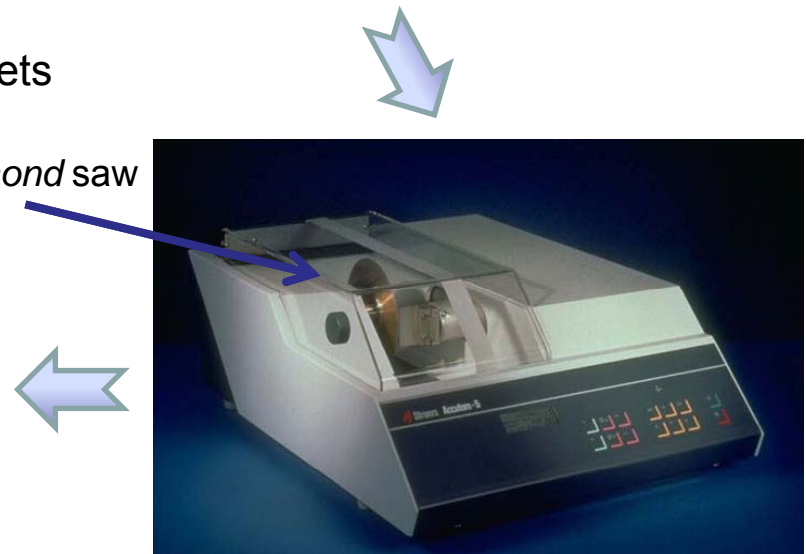


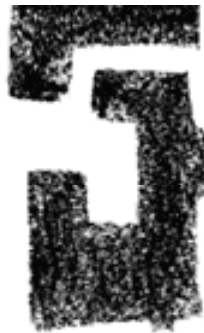
Pressed into pellets



Rectangular bars

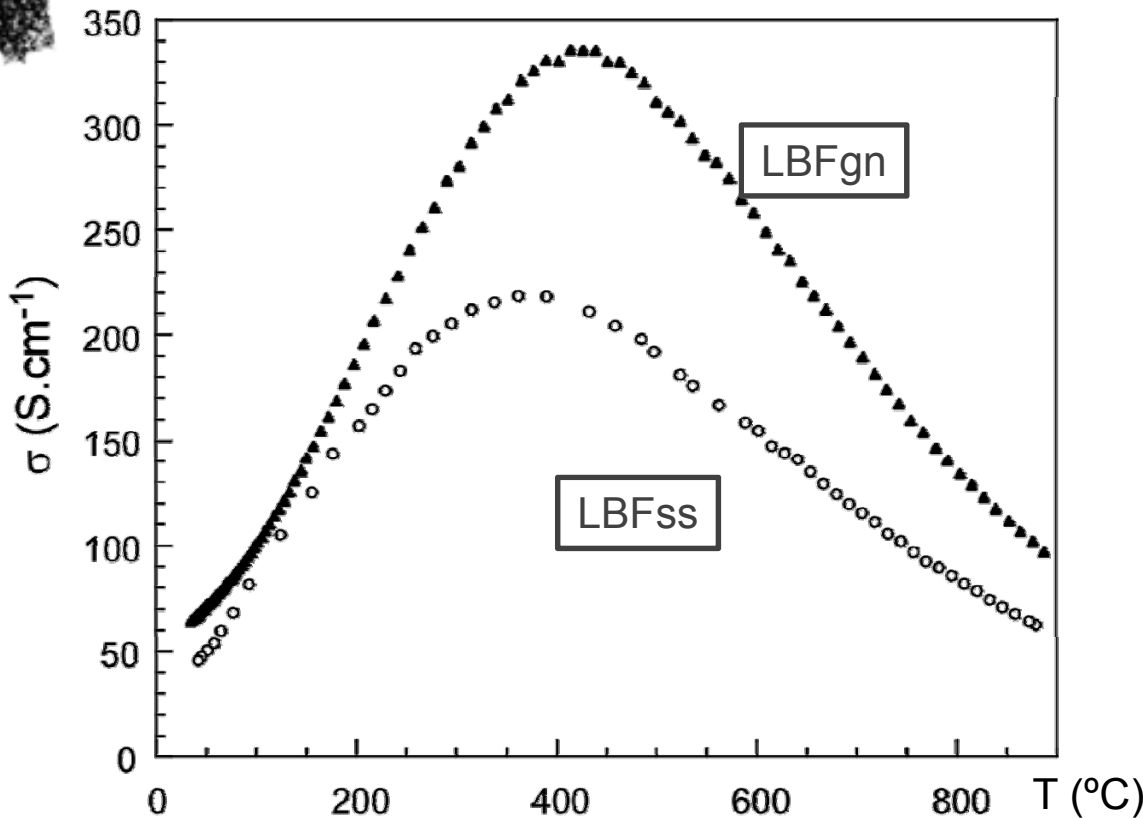
Diamond saw





## Electrical conductivity

Four-point method 30-900°C in air

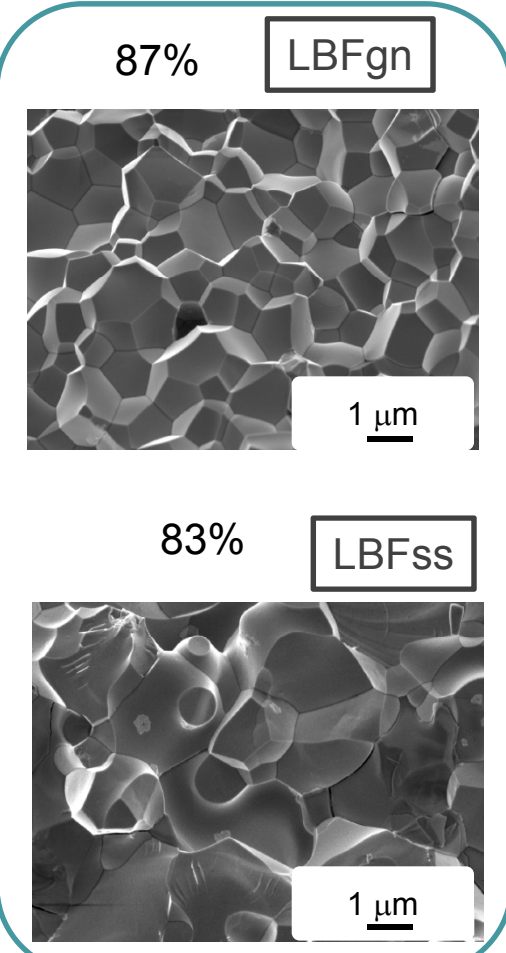


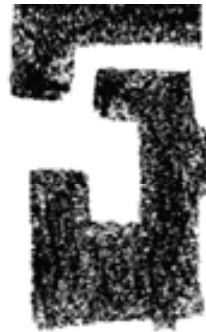
The electrical conductivity measured by the four-point method increases with increasing temperature, goes through a broad maximum and then decreases  $\Rightarrow$  hopping of p-type small polarons.

LBFgn sample presents higher values of electrical conductivity.

## Characterization

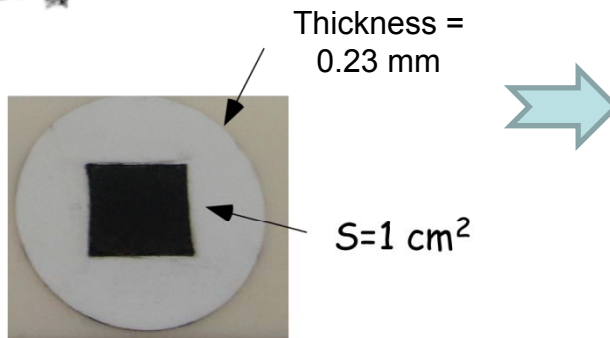
SEM micrographs



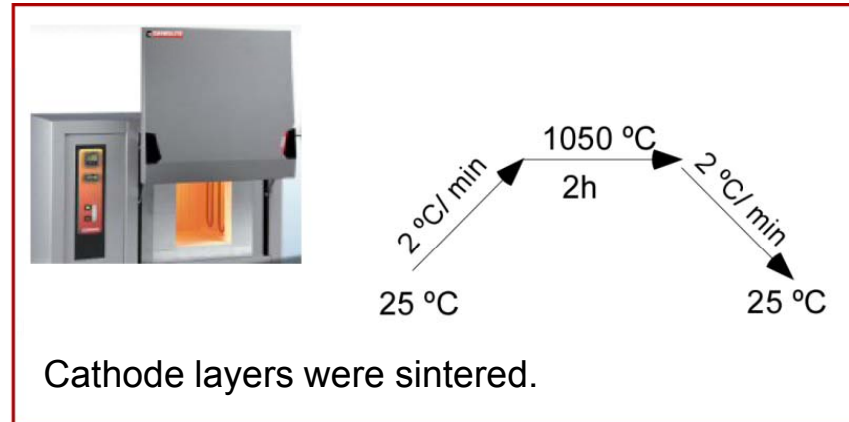


## Electrochemical impedance spectroscopy (EIS)

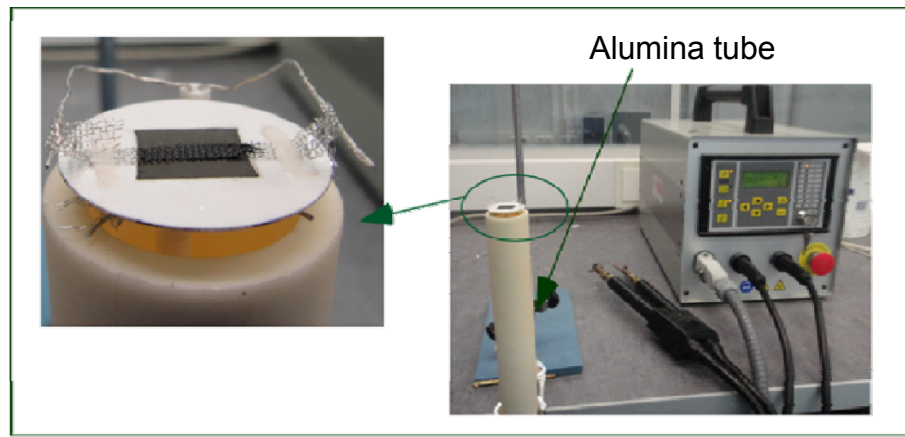
### Characterization



The cathode layers were deposited onto both sides of the electrolyte, 8YSZ, by wet colloidal spraying.



Impedance measurements of the symmetric cells were performed in air at 700 and 800°C.



Impedance measurements of the cathode suspensions were performed on symmetrical cells, with AC signal amplitude of 10 mV over the frequency range of 10<sup>6</sup>-0.01 Hz at 700 and 800°C.



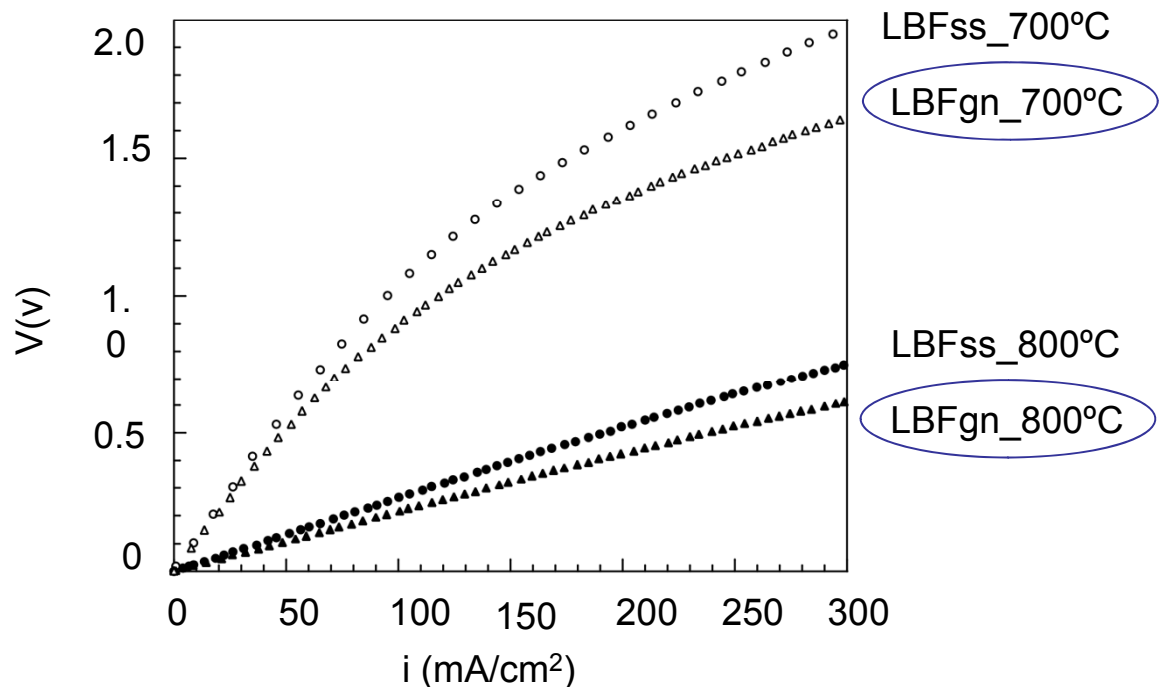


## Electrochemical impedance spectroscopy (EIS)

Characterization

Current–voltage ( $I/V$ ) curves at 700 and 800°C.

Better performance  
for LBFgn

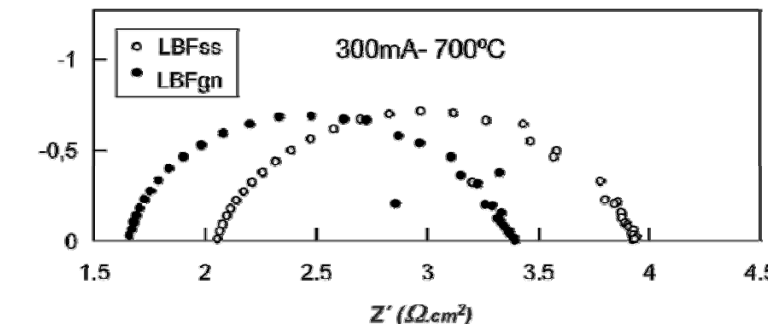
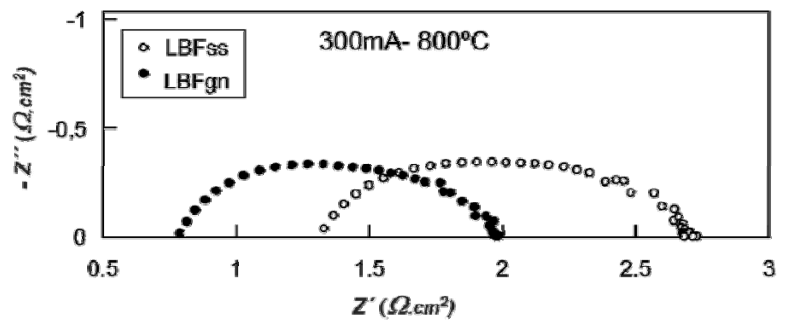
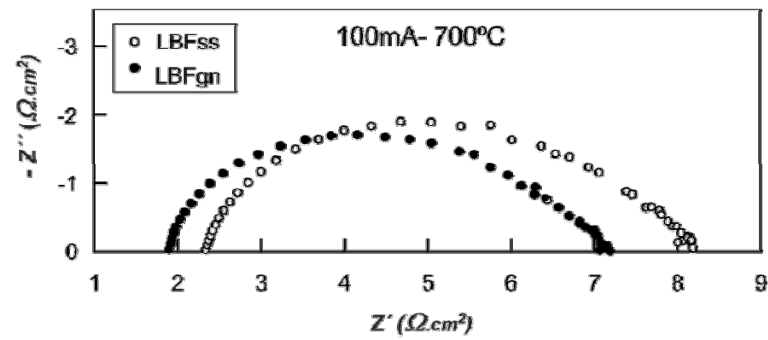
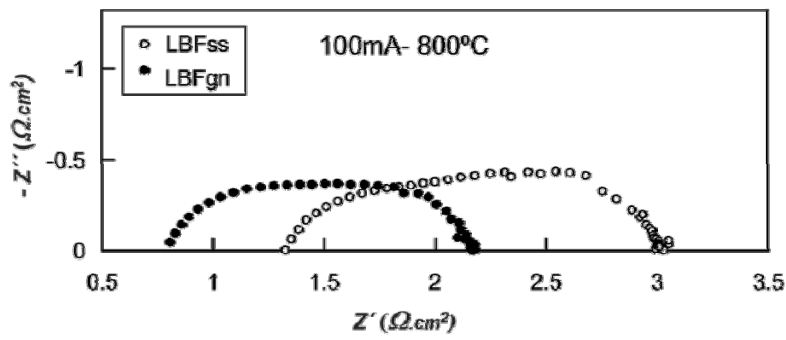
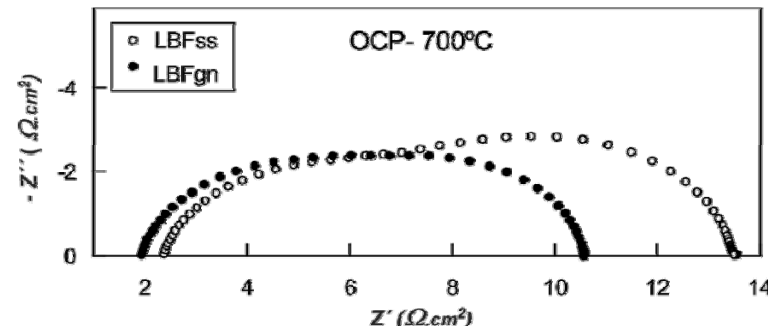
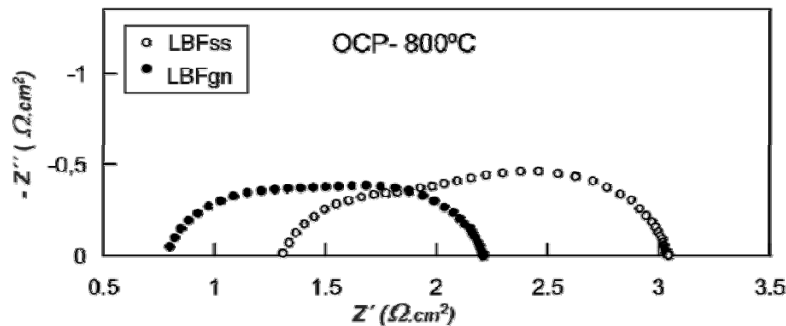




# Electrochemical impedance spectroscopy (EIS)

## Characterization

The impedance spectra of the two compounds obtained at OCP, 100 and 300 mA at 800 and 700°C.





## Electrochemical impedance spectroscopy (EIS)

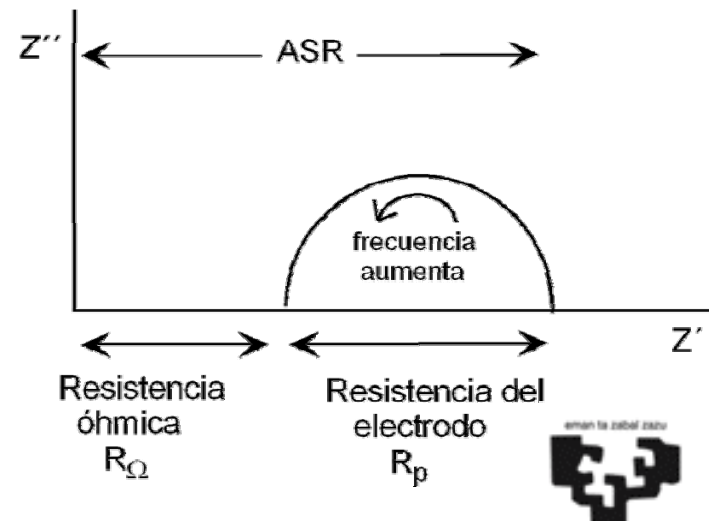
## Characterization

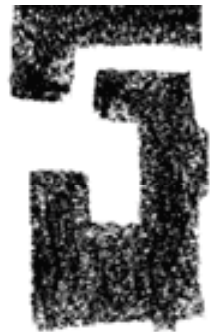
Sample	T(°C)	R <sub>Ω</sub> (Ω.cm <sup>2</sup> )			ASR(Ω.cm <sup>2</sup> )			R <sub>p</sub> (Ω.cm <sup>2</sup> )		
		OCP	100mA	300mA	OCP	100mA	300mA	OCP	100mA	300mA
LBFss	800	1.31	1.32	1.30	3.04	3.00	2.71	1.74	1.68	1.41
LBFgn	800	0.78	0.78	0.79	2.21	2.16	2.00	1.43	1.38	1.21
LBFss	700	2.35	2.33	2.04	13.58	8.09	3.93	11.16	5.75	1.89
LBFgn	700	1.93	1.88	1.65	10.52	7.16	3.37	8.59	5.28	1.72

The polarization resistance increases with decreasing the temperature due to lower mobility of the ions.

Polarization resistance values are similar being slightly lower for the LFBgn sample.

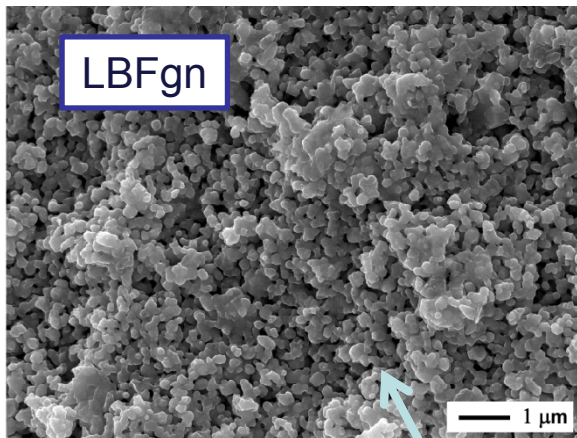
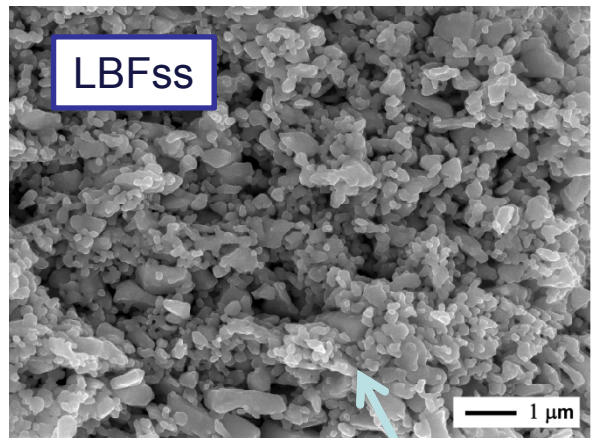
Ohmic resistance values are lower in the case of the compound prepared by glycine-nitrate route.





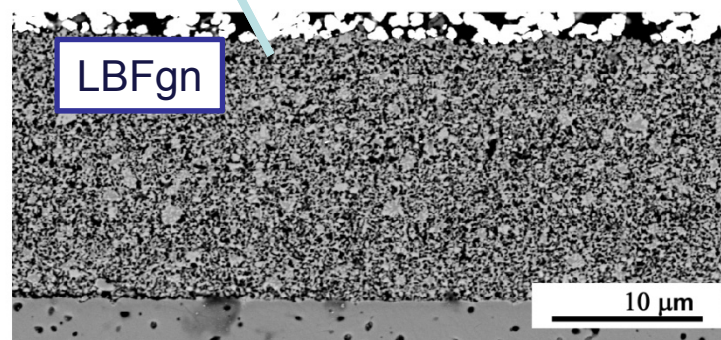
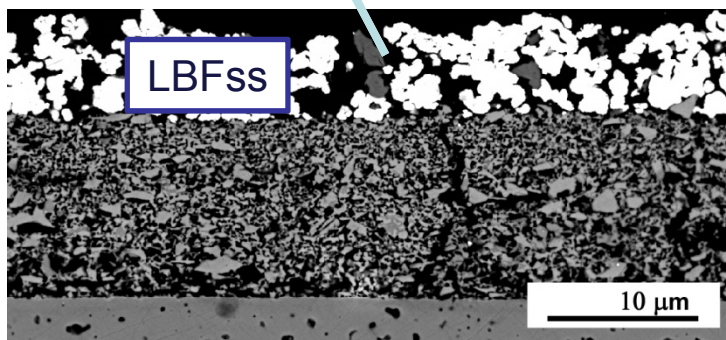
## Scanning electron microscopy (SEM)

## Characterization



The higher value of ohmic resistance of the LBFss sample is attributed to a possible worse contact between the cathode and the electrolyte. This is maybe due to the bigger particle size of the LBFss powder.

Cross-sectional  
microstructures



Pt

Cathode

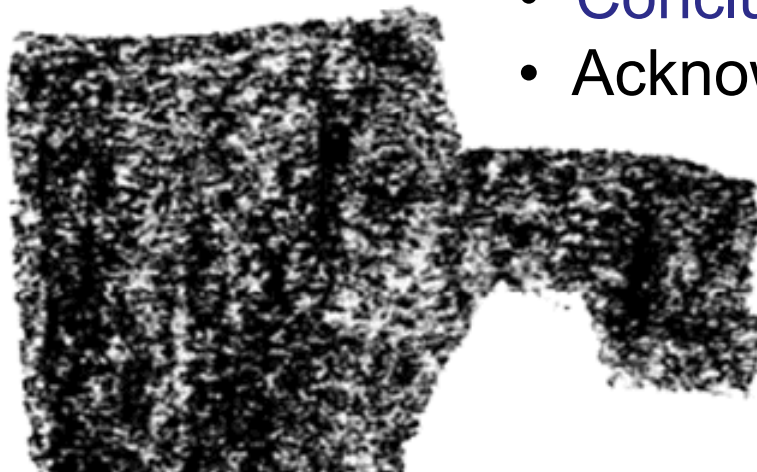
Electrolyte



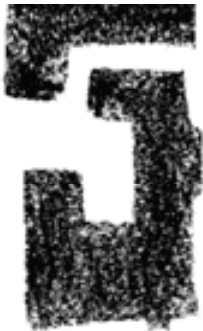


## Contents:

- **Introduction**
  - Solid oxide fuel cells
  - Perovskites
- **Experimental preparation**
  - Solid state reaction
  - Glycine nitrate combustion process
- **Characterization**
  - Structure (X-ray and neutron diffraction )
  - Microstructure
  - Bulk conductivity
  - Thermal expansion coefficient
  - Polarization resistance
- **Conclusions**
- **Acknowledgments**



## Conclusions



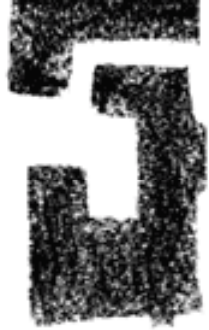
$\text{La}_{0.5}\text{Ba}_{0.5}\text{FeO}_3$  compound has been obtained by ceramic and glycine nitrate methods .

At room temperature, both compounds show cubic symmetry (S.G:  $P\ m\text{-}3m$ ), being the oxygen vacancy content the main structural difference observed. However, at high temperature the oxygen content of the samples become similar.

The compound obtained by glycine-nitrate method presents the most suitable characteristics as cathode material: fine particle sizes, higher surface areas and the lower area specific resistance values at 700 and 800°C.

Therefore, it can be concluded that the glycine-nitrate process is a more appropriate technique for preparing perovskite cathodes.





## Acknowledgements

This research has been funded by:

Dpto. Educación, Política Lingüística y Cultura of the Basque Goverment (IT-630-13).

Ministerio de Economía y Competitividad (MAT2013-42092-R).

The authors thank SGIker (UPV/EHU) technical support.

K. Vidal thanks UPV/EHU for funding.



**Thank you very much for your attention**



Universidad  
del País Vasco      Euskal Herriko  
                              Unibertsitatea

